

Study of time over threshold method using simulations and experimental verification

Christiaan Brits

Dr. Vyacheslav Mikhailovich Golovatyuk

JINR Summer student Program 2015
Dubna, Russia 2015

Abstract

The time over threshold method is used in the NINO amplifier chip in time of flight measurements in the MPD detector. For the TOF measurements MRPC detectors are used. A signal coming from the MRPC is simulated and the effects noise has on the time resolution of the time over threshold method is studied using simulations. Using a signal and noise generator the effects of the noise on the time resolution in the time over threshold method is experimentally investigated.

Contents

- Introduction
 - Multi-Purpose Detector (MPD)
 - Multigap resistive plate chamber detector (MRPC)
 - Time over threshold method
- Simulation
 - Setup
 - Noise generation
- Simulation results
 - Sinusoidal noise
 - White noise
 - Variance of time distribution
- Experiment
 - Setup
 - Data analysis method
 - Results
- Conclusion
- References

Introduction

MPD

The MPD is designed as a 4π -spectrometer capable of detecting charged hadrons, electrons and photons in heavy-ion collisions in the energy range of the NICA collider [1, 2]. To reach this goal, the detector will include a precise 3-D tracking system and a high-performance particle identification system based on time-of-flight measurements and calorimetry. At the design luminosity, the event rate in the MPD interaction region is about 6 kHz. The total charged particle multiplicity exceeds 1000 in the most central Au+Au collisions at $\sqrt{s_{NN}} = 11$ GeV.

The multi-purpose detector consist of three different parts: the central detector (CD) and two forward spectrometers FS-A and FS-B. The spectrometers will be positioned along the beam line symmetrically with respect to the center of the MPD. The CD has a barrel part and two end caps positioned inside the magnetic field. The barrel part has various detector systems surrounding the interaction point. The barrel part will reconstruct and identify both charged and neutral particles over pseudo rapidity range $|\eta| < 1.2$. The end caps will do precise tracking over pseudo rapidity range $1.2 < |\eta| < 2$. FS-A and FS-B situated on both sides of the MPD barrel will cover the pseudo rapidity range $2 < |\eta| < 3$.

The barrel part consists of trackers and a particle identification system. The principle tracker is the time projection chamber (TPC) supplemented by the inner tracker (IT). These sub detectors will provide precise track finding, momentum determination, vertex reconstruction and pattern recognition. The inner tracker is a silicon strip detector representing a barrel of double sided position sensitive layers around the interaction region. The energy loss measurements in the TPC gas will give addition capability for particle identification in low momentum regions.

The high performance time-of-flight (TOF) system must be able to identify charged hadrons and nuclear clusters in the broad rapidity range and up to total momentum of 2 GeV/c. The fast forward detectors (FD) will provide the TOF system with the start signal.

The electromagnetic calorimeter (EMC) is used to identify electrons, photons and measure their energy with high precision. The high granularity of the EMC together with excellent energy resolution and good timing performances will enhance the overall efficiency and particle identification capabilities of the MPD detector.

Two straw tube trackers (ECT) are located on both sides of the TPC along the z-axis. The current design includes wheel-like tracking detectors based on straw tubes supplemented by two cathode pad chambers (CPC). The ECT is designed to provide tracking information for particles travelling at small radii and for which the TPC has poor reconstruction ability. Thus a supplementary principle is exploited for tracking of the charged particles in the pseudo rapidity region up to $\eta = 2$. It allows a precise definition of an azimuthal angle for charged tracks and momentum reconstruction with a sufficient precision. Particles emitted in very forward/backward directions are detected by fast forward detectors (FD), beam-beam counters (BBC) and zero degree calorimeters (ZDC). They are used for trigger definition, centrality determination and reconstruction of the position of the interaction point. The general design of the MPD is shown in figure 1. [1]

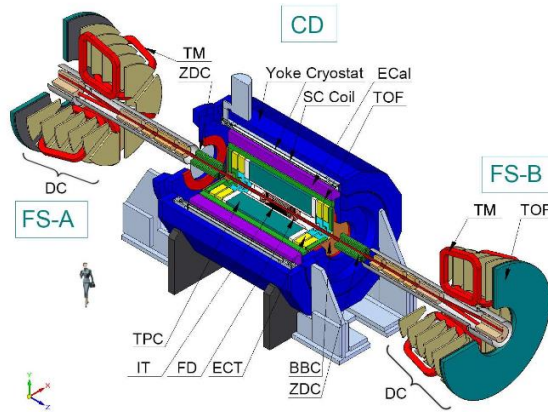


Figure 1 General view of the MPD detector [1]

Multigap resistive plate chamber (MRPC)

The main detector in the TOF system is the MRPC. A scheme of the MPD TOF detector is presented in figure 2. The MRPC detector consists of two stacks with 5 gas gaps each. As resistive electrodes common float glass is used. The resistive electrodes is used to quench the streamer and prevent a spark breakdown. The outer glass electrodes have thickness 0.55mm. The internal glass electrodes have thickness 0.4mm. The fishing line, which is used as a spacer, defines the 220 μ m gap between all resistive electrodes. The outer part of the external glass electrodes is covered by conductive paint with surface resistivity about 2 – 10 M Ω /cm to which a high voltage is applied. All internal glasses are left floating. The voltage of the internal plates appears due to the flow of electrons and ions created in the gas gaps. An important feature of the double-stack “strip” detector is that the internal strips of two different stacks are separated by a 5-mm panel Honeycomb. This ensures the symmetry between the two stacks, and provides the equal speed of signals on the anode and cathode strips and as a result prevents the dispersion of the signal. [3]

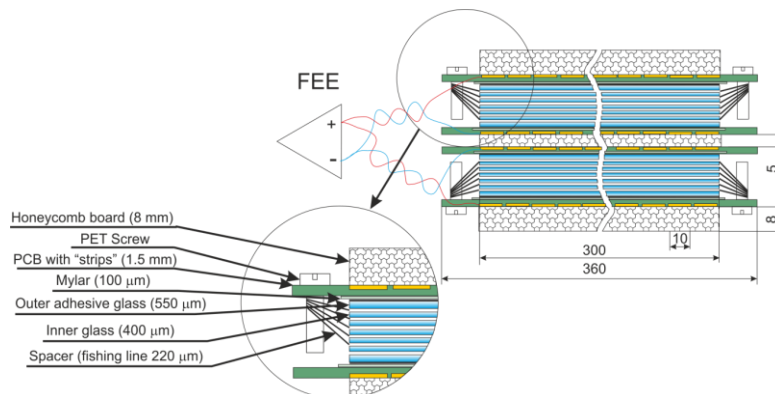


Figure 2 Sectional view of double stack strip MRPC for TOF MPD [3]

The MRPC is filled at 2-3mbar with:

- 90% C₂H₂F₄
- 5% SF₆
- 5% i-C₄H₁₀.

When a particle goes through the detector it creates an electron ion pair in the gas. In the presence of an electric field (100kV/cm in the MRPC) the electrons gets accelerated to the anode and the positive ions gets accelerated to the cathode. The electrons will collide with other particles creating an avalanche of

electron ion pairs as shown in figure 3. The resistive plates will then absorb the avalanches, however the plates are transparent to the electric field generated by the moving electrons. The electric field then generates a signal in the readout electrodes. So the total signal is the sum of the signals from all gaps. The time jitter of the signal depends on the individual gap width. This means more gaps give a higher efficiency and smaller gaps give a better time resolution. [4]

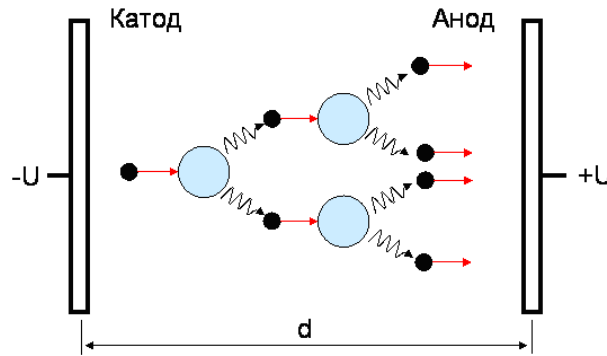


Figure 3 discrete avalanches in a RPC [11]

Time over threshold method

The signal coming from the detector is amplified by a NINO application-specific integrated circuit (ASIC). The NINO ASIC is developed in 0.25 micron CMOS technology developed by the CERN LAA project, which combines a fast amplifier, discriminator and stretcher. The NINO ASIC chip is shown in figure 4.

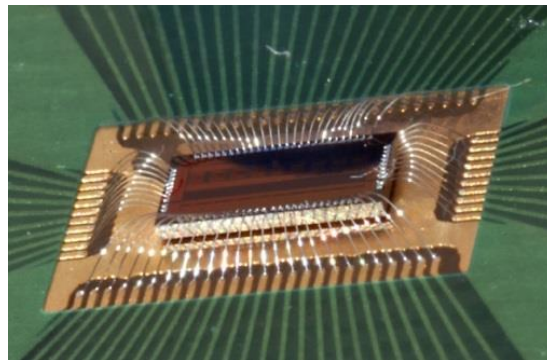


Figure 4 NINO ASIC chip

The NINO output pulse width is somewhat dependent on the MRPC pulse height. Thus the integral of the pulse (charge) can be obtained by measuring the pulse width. The pulse width is defined as the time difference between when the pulse goes below the threshold (leading edge) and the time it returns above the threshold (trailing edge), as shown in figure 5. Time correction using ToT pulse width is called the “Time-Over-Threshold” method [5]. Because this method requires only time information it can simplify and reduce the cost of readout electronics. The dependence of the width of the ToT pulse on the input charge of the NINO chip is shown in figure 6.

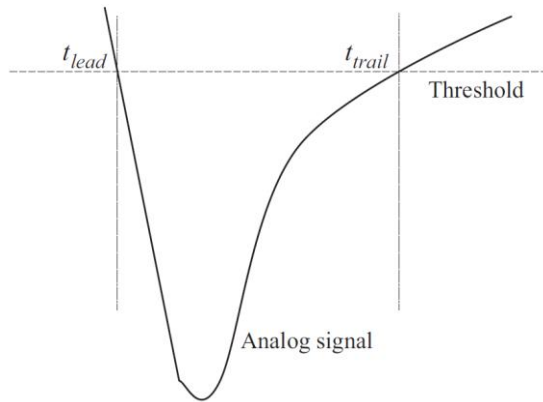


Figure 5 The time over threshold method [7]

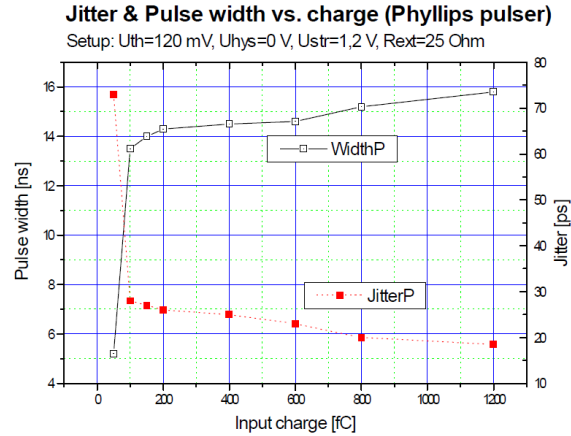


Figure 6 Input charge and pulse width dependence [7]

Recent studies at CERN SPS has shown a peculiar structure in the reconstructed distribution of the ToT (see figure 7). The structure can be explained by the superposition of sinusoidal noise added to the PMT signal [7]. This has led to the investigation of the ToT method in the presence of noise with the MRPC detectors.

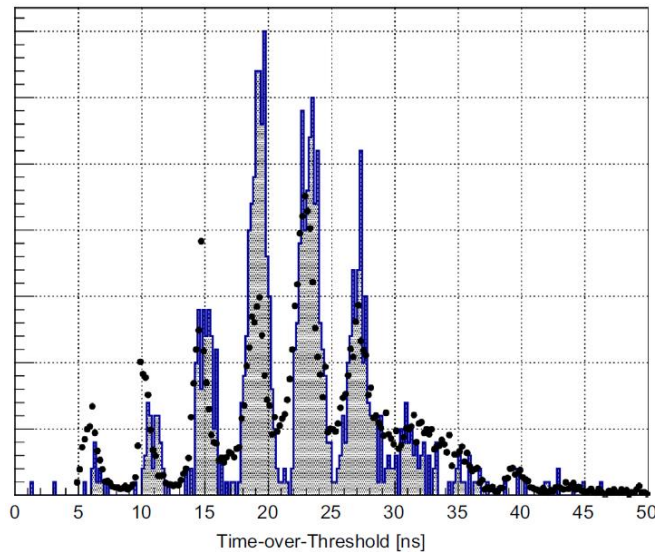


Figure 7 Comparison between the measured (dots) and the simulated (histogram) ToT [7]

Simulation

Setup

The signal coming from the detector is amplified by the NINO chip so that the charge and corresponding width can be calculated. The path of the pulse is shown in figure 8. The signal coming from the detector is simulated as a Gaussian function with amplitude 20-60mV (333fC-1000fC on 50 Ohm resistor) and variance 0.33ns. This gives a 2ns signal.

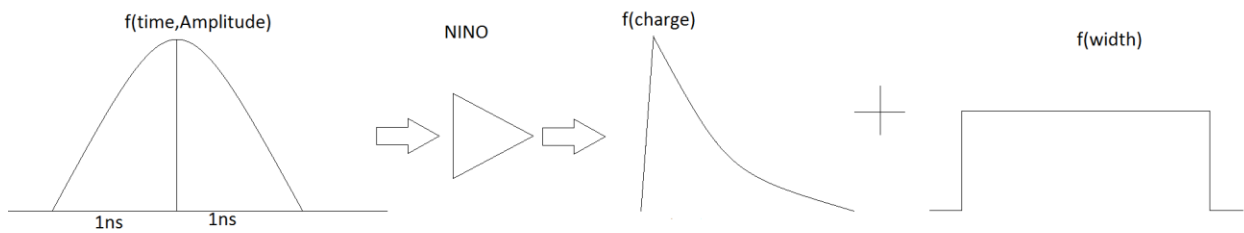


Figure 8 the pulse coming from the detector and going through the NINO chip

The charge of the pulse is the area beneath the pulse. The width of the pulse is then calculated by the parameterized functions of Figure 6. In order to find the parameterized function of figure 6 it was fit with three different functions as shown in Figure 9.

- 0 – 100 : $width = -3.5 + 0.17 \times charge$
- 100 – 200 $width = 8.4882 + 1.0919 \times \log(charge)$
- 200 – 1200 : $width = 13.824 + 0.0016182 \times charge$

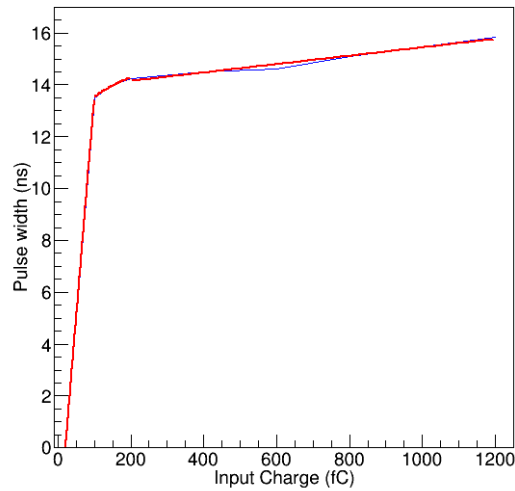


Figure 9 fit of input charge with the pulse width

Once the width has been calculated the time of the pulse can be calculated through:

$$time = 74.664 * \exp\left(\frac{width}{2.6315}\right) - 0.23854$$

The time and width of a pulse related to this equation is shown in figure 10.

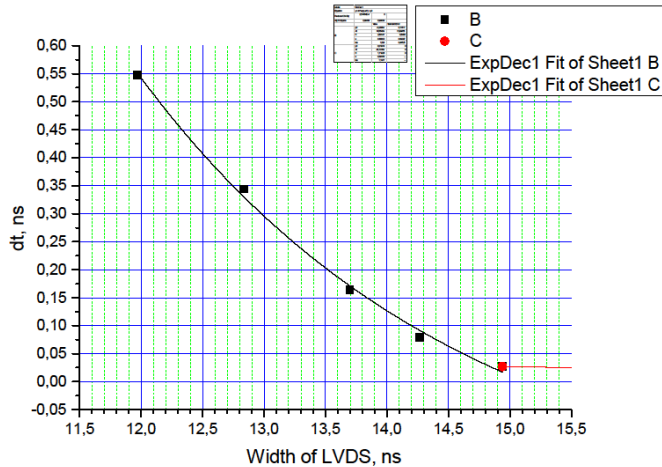


Figure 10 the time and width dependency

Calculating the difference between the signal with and without noise the time distribution can be measured. Two different types of noise was considered, sinusoidal based noise and Gaussian white noise, as shown in Figure 11.

Noise generation

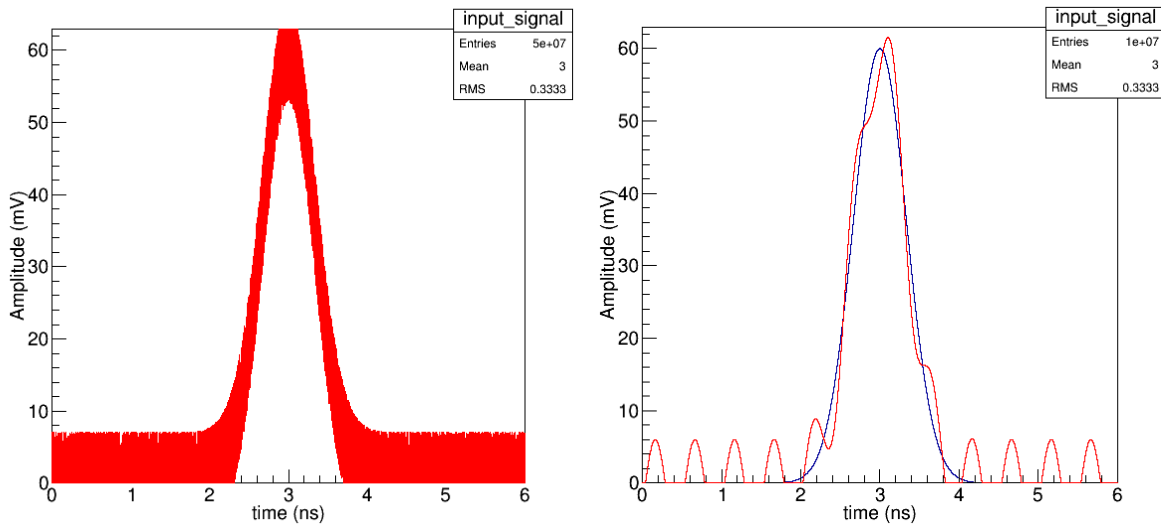


Figure 11 an example of Gaussian white noise (left) and sinusoidal noise (right)

The sinusoidal noise was defined as:

$$y = A \times \sin\left(2\pi f + \frac{\phi}{2\pi f}\right)$$

Where A is the amplitude of the noise, f the frequency and ϕ the phase. The white noise was generated using the box-muller method. The box-muller method uses inverse transformation to turn 2 uniformly distributed random numbers into 2 unit normal random numbers with mean 0 and variance 1. [9, 10]

$$y1 = \sqrt{-2 \log(R1)} \times \cos(2\pi R2)$$

$$y2 = \sqrt{-2 \log(R1)} \times \sin(2\pi R2)$$

Where R1 and R2 are 2 uniformly distributed random numbers and $R1 \neq 0$. The mean and variance can easily be modified by:

$$y1' = mean + \sqrt{variance} y1$$

The frequency, phase, signal and noise amplitude is varied respectively and the effect this has on the width and time distribution is studied. When the parameters are not varied they are kept constant at:

- Resistance at 50Ω.
- Signal amplitude at 60mV (charge at 1000fC).
- Noise amplitude at 10% of signal amplitude.
- Phase at 0ns.
- Frequency at 2GHz.

Simulation results

Sinusoidal noise:

In figure 12 the phase is randomly chosen between 0-1ns while the other parameters are kept constant:

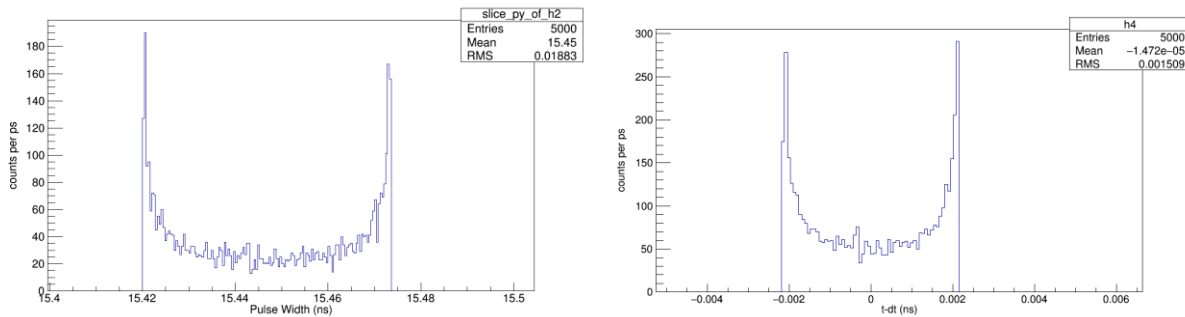


Figure 12 the width (left) and time (right) distribution resulting from the phase being randomly varied between 0-1ns

The width distribution has a RMS of 18.83ps and the time distribution has a RMS of 1.509ps. Two peaks can be seen in the width and time distribution at the ends of the distribution. The time between the peaks in the time distribution is 4ps. The time between the peaks depends on the frequency of the noise. If the frequency is kept constant at 1GHz the time between the peaks become 8ps, see figure 13.

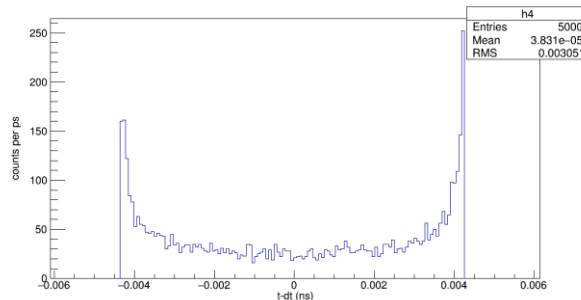


Figure 13 time distribution when the frequency is kept constant at 1GHz

If the phase is varied with another parameter the two distinct peaks disappear, see Figure 18. This means that in an experiment where the signal amplitude, noise amplitude, phase and frequency vary the two

peaks will not show up in the data. In figure 14 the frequency of the sinusoidal noise is varied from 0-2GHz in steps of 4MHz while the other parameters are kept constant:

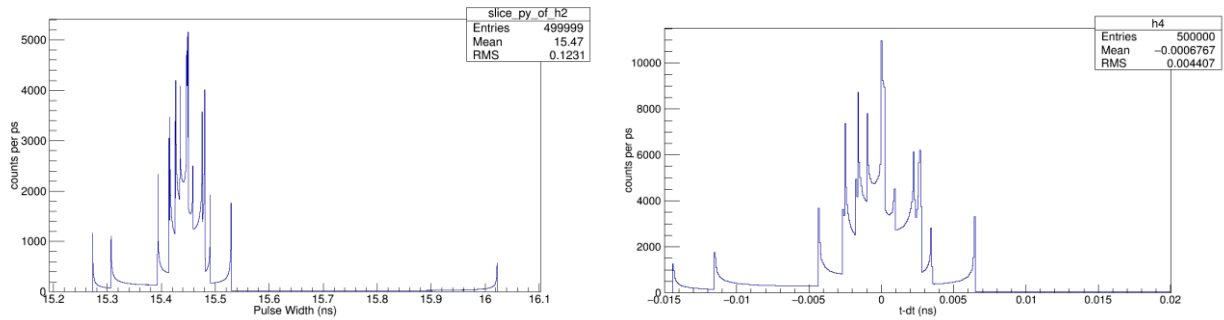


Figure 14 the width (left) and time (right) distribution resulting from a varied frequency from 0-2GHz in steps of 4Hz.

The width distribution has a RMS of 0.1231ns and the time distribution has a RMS of 4.407ps, however many peaks can be observed in the distributions. The amount of peaks depends on the frequency, a higher frequency gives more peaks and a lower frequency gives less peaks. If the frequency and another parameter is varied at the same time, the peak structures disappears or becomes less noticeable. As with the phase, the peak structures should not be visible, or at least not very distinct, in experimental data. In figure 15 the noise amplitude is varied from 0-10% of the signal amplitude:

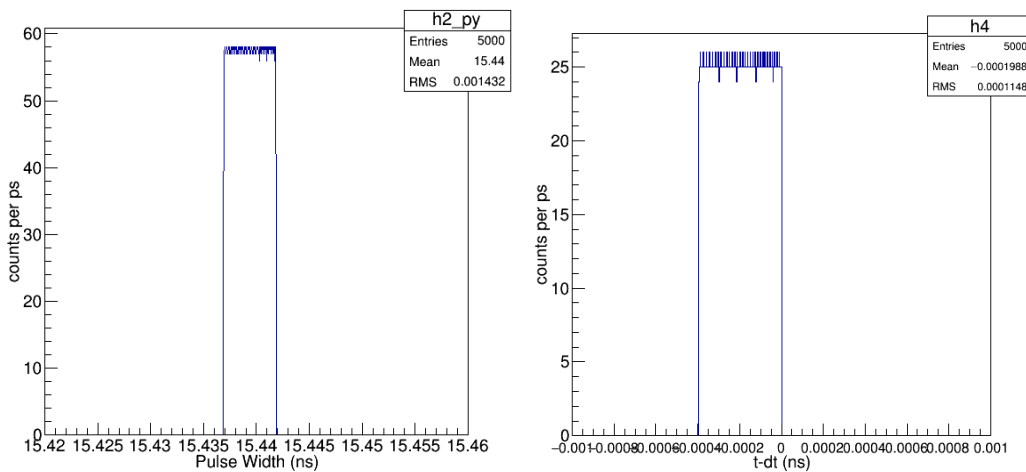


Figure 15 the width (left) and time (right) distribution obtained from a varied noise amplitude of 0-10% of the signal amplitude

A noise amplitude of 10% of the signal amplitude is expected in an experimental situation. The noise amplitude of 10% of the signal amplitude has little influence on the time and width distribution. The time distribution has a RMS of 0.1148ps and the width distribution has a RMS of 1.432ps. In figure 16 the signal amplitude is varied between 20mV and 60mV with a uniform and Gaussian distribution:

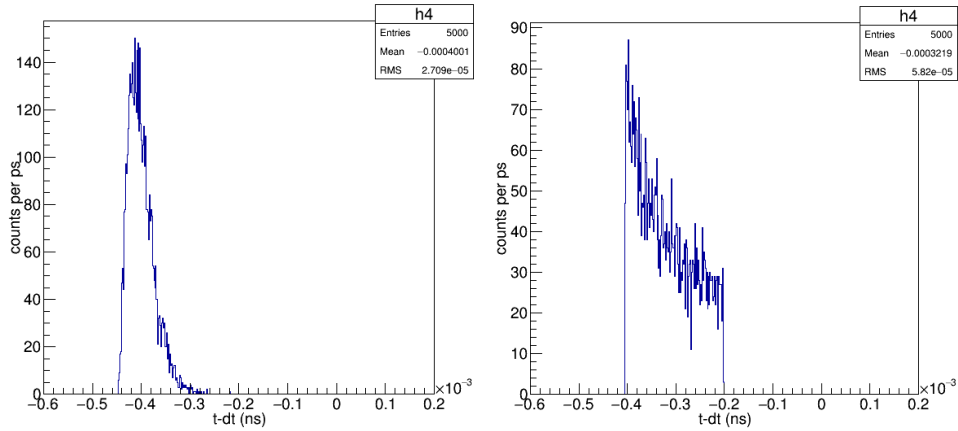


Figure 16 the time distribution from varying the signal amplitude with a Gaussian distribution (left) and a uniform (right) distribution.

The Gaussian distribution has a RMS of 2.709×10^{-5} ns and the uniform distribution has a RMS of 5.82×10^{-5} ns. The signal amplitude has little influence on the time distribution.

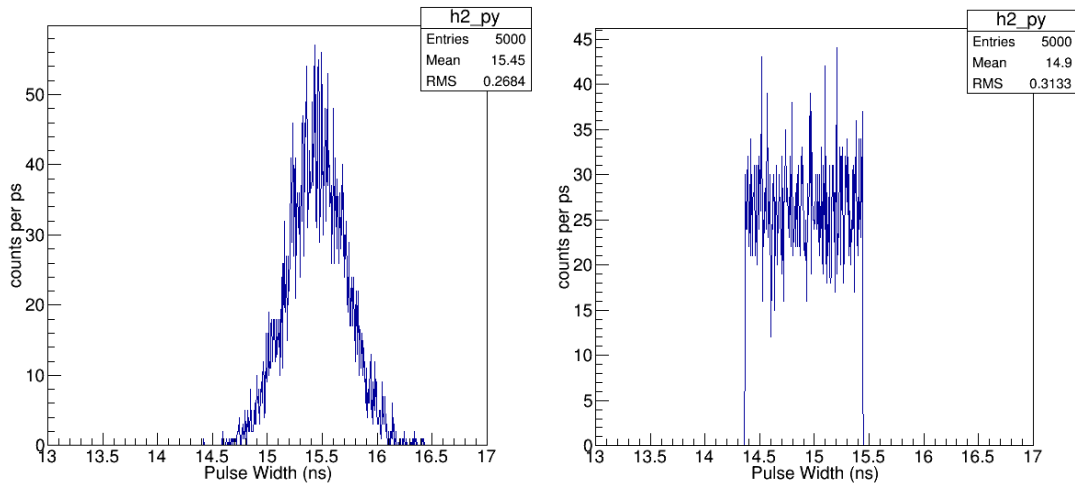


Figure 17 the width distribution from varying the signal amplitude with a Gaussian (left) distribution and a uniform (right) distribution.

The Gaussian distribution has a RMS of 0.2684ns and the uniform distribution has a RMS of 0.3133ns. In figure 18 the amplitude is varied from 20-60mV, the noise from 0-10%, the phase from 0-1ns and the frequency from 0-2 GHz:

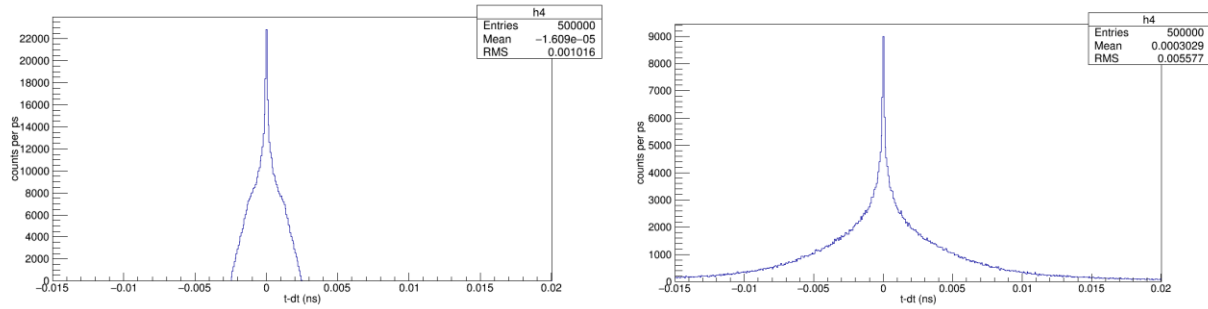


Figure 18 time distribution when all the parameters are varied with Gaussian (right) and uniform (left) distributed parameters.

The peak structures resulting from the phase or frequency seems to be suppressed or not noticeable. It can be concluded that the peak structures observed in Figures 12 and 14 should not affect the experimental data. The time distribution with uniform distributed parameters has a RMS of 1.016ps and the time distribution with Gaussian distributed parameters has a RMS of 5.577ps.

White noise

In figure 19 the white noise amplitude is uniformly varied between 0-10% and the signal amplitude is varied uniformly between 20-60mV:

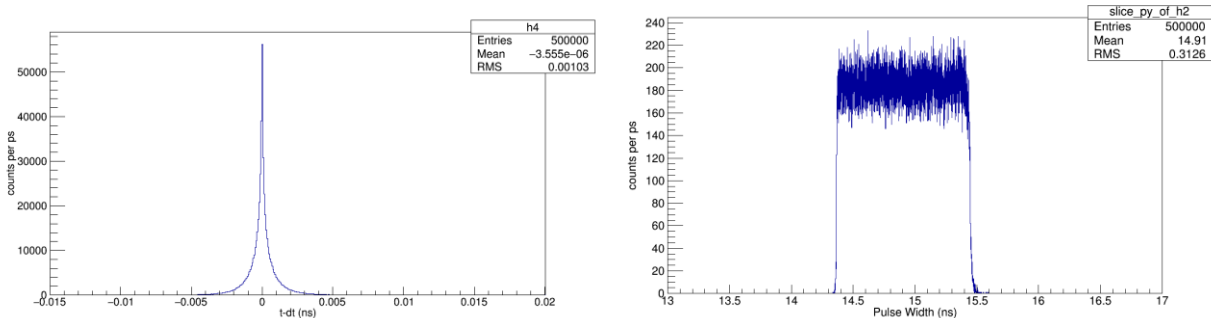


Figure 19 the time (left) and width (right) distribution of white noise with varying noise amplitude

The time distribution of white noise has a RMS of 1.03ps and the width distribution has a RMS of 0.3126ns. In order to further see the effect the noise has on the time distribution the variance of the time distributions are calculated.

Variance of time distribution

The variance and variance error of the time distribution is then calculated and plotted with the frequency. For white noise the amplitude is varied randomly between 20-60mV and the noise amplitude is randomly varied between 0-10% and 0-50% of the signal amplitude respectively:

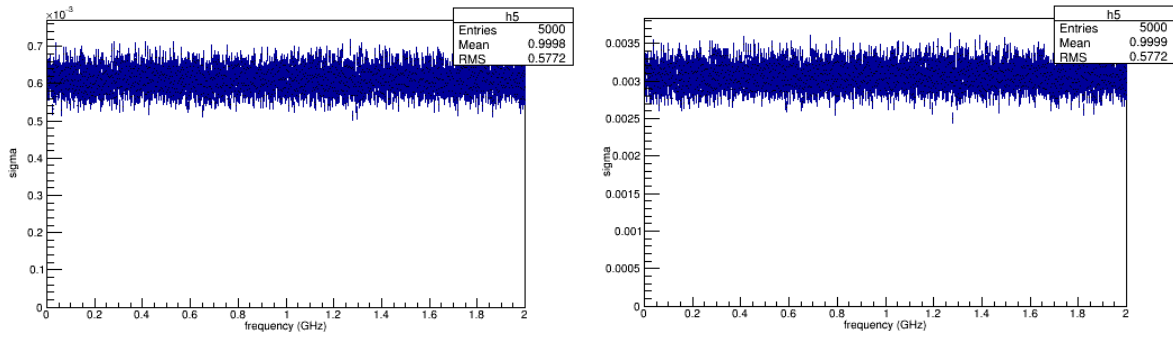


Figure 20 Variance for the time distribution of white noise at 10% (left) and 50% (right) noise amplitude.

The figure on the left has 10% noise amplitude and the figure on the right has 50% noise amplitude. The effects of the white noise is very small and the variance remains at 3ps for 50% noise amplitude and 0.6ps for 10% noise amplitude. For the sinusoidal noise the amplitude is varied randomly between 20-60mV, the noise amplitude is randomly varied between 0-10% and 0-50% respectively, the frequency is varied from 0-2GHz and the phase is randomly varied from 0-1 Period:

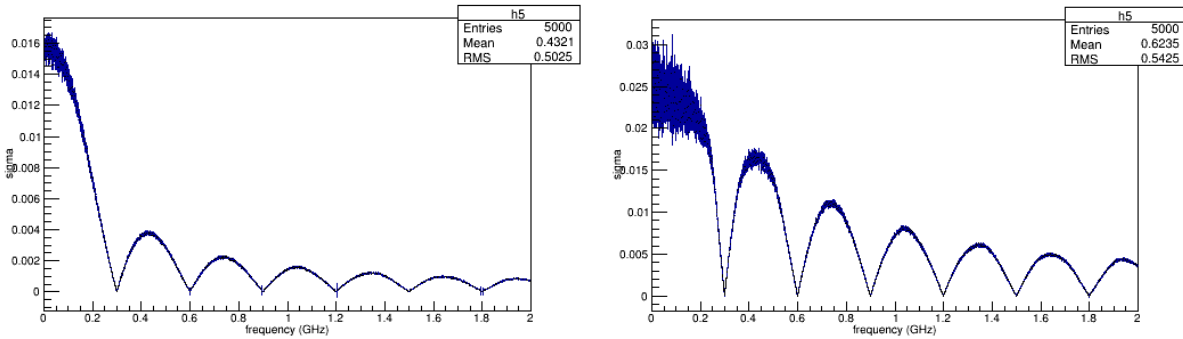


Figure 21 variance of the time distribution with sinusoidal noise at 10% (left) and 50% (right) noise amplitude.

The figure on the left has 10% noise amplitude and the figure on the right has 50% noise amplitude. The sinusoidal noise has a higher variance than the white noise. For 50% noise amplitude the variance can have a maximum value of 27ps and for 10% noise amplitude the maximum value is 15ps. A period of 300MHz is observed in the variance in figure 21. This occurs because the pulse is integrated over 3ns resulting in the 300MHz period. This means every 300MHz the sinusoidal noise has very little effect on the pulse.

The higher the frequency of the noise, the better the time resolution will be. When integrating noise over many periods the average noise should be 0. By increasing the frequency the amount of periods being integrated increases and the average effect of the noise gets closer to 0. This is also why the error of the variance gets smaller the higher the frequency is.

Experiment

Setup

Using a signal generator (A) a 2 ns Gaussian signal is generated. This signal is then split into two parts, one part going to the oscilloscope (E) and the other part going to the differential splitter (G). The

differential splitter has one input channel and 4 output channels. Normally the differential splitter takes the input signal and produces 4 similar signals of which 2 is positive and 2 negative. The amplitude of the output pulses depends on the power supply (C) of this circuit. When the pulse from the sinusoidal noise generator (D) is attached to the power supply, the amplitude of the output signal is changed according to the sinusoidal pulse, thus adding the noise to the signal. This is shown in figure 22.

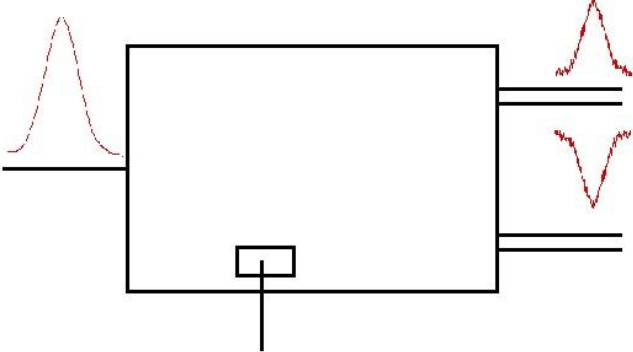


Figure 22 Diagram of the differential splitter

Two of the signals from the differential splitter go directly to the oscilloscope and the other two goes to the NINO amplifier and then the oscilloscope. A diagram of the setup is shown in Figure 23 and pictures of the setup is shown in figure 24.

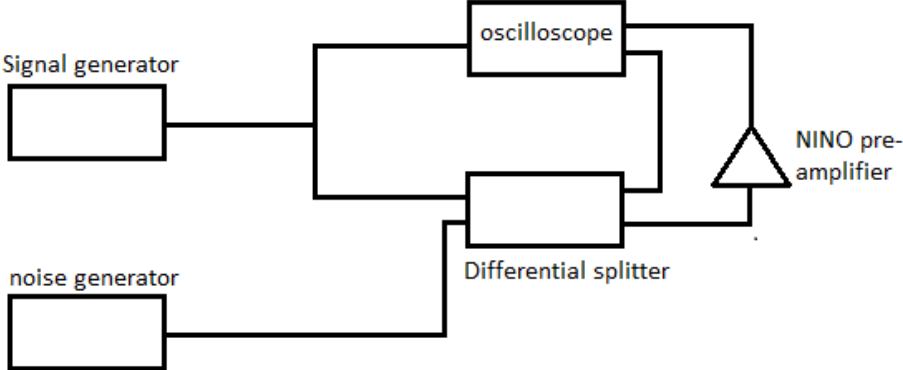


Figure 23 diagram of the experimental setup

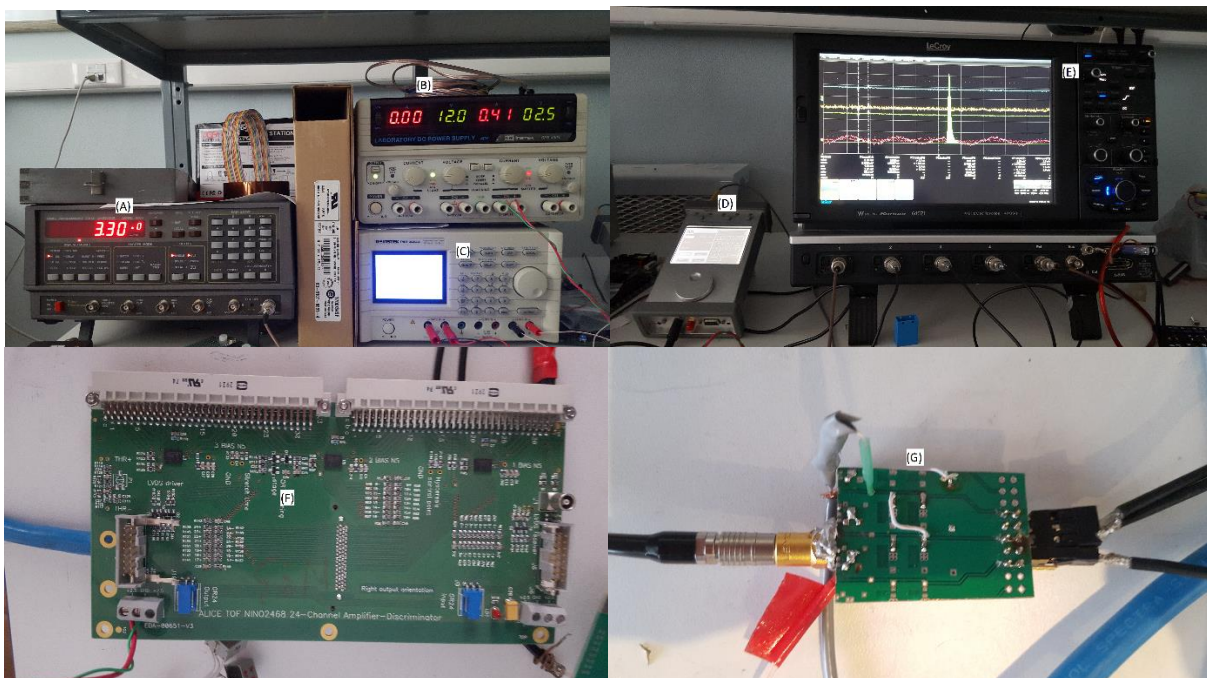


Figure 24 Experimental setup, (A) is the Gaussian signal generator, (B) is the amplifier power supply (C) is the differential splitter power supply, (D) is the sinusoidal noise generator, (E) is the oscilloscope, (F) is the NINO amplifier and (G) is the differential splitter

Using this setup data is taken with varying noise amplitude from 100-1000mV (where 100mV is 10% of the signal amplitude) and a constant frequency of 1GHz. Data is also taken with varying frequency from 0MHz to 1GHz with a constant noise amplitude of 100mV.

Data analysis method

Figure 25 shows the different signals generated. The red signal is the primary signal with noise and the yellow signal is the primary signal without noise. The integral of these signals are related to the charge produced in the MRPC by a charged particle. The green and blue signals are the signals coming from the NINO amplifier. The width of these signals are related to the charge from the MRPC.



Figure 25 the different signals investigated: the primary signal without noise (yellow), the primary signal with noise (red) and the signals coming from the NINO amplifier (green and blue)

Traces of these signals are used for data analysis. In order to find the time distribution off the data 3 fits were taken as shown in Figure 26. The start time is found on the signal without noise, when the fit of the leading edge (function 2) and the fit of the baseline (function 1) cross. The stop time is found on either of the pulses coming from the NINO amplifier, when the fit of the leading edge (function 3) goes through zero.

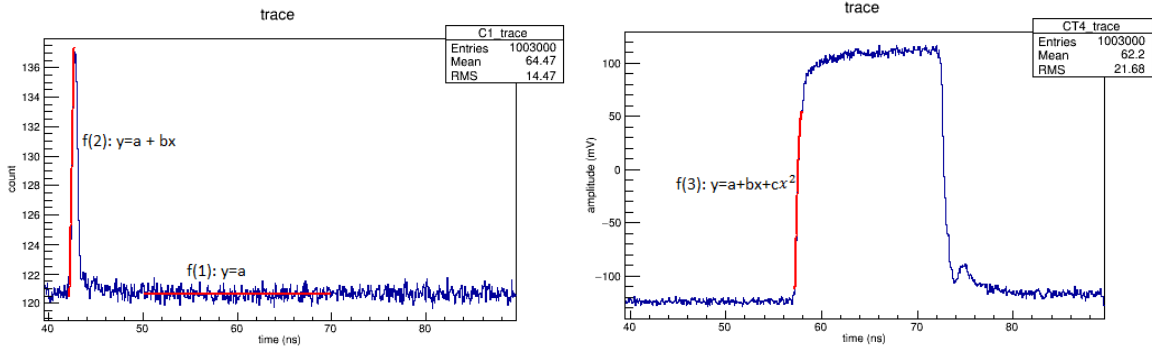


Figure 26 fits for time correction to determine the start and stop time

When the width distribution is plotted against this time distribution time correction can be done. Taking the mean value of the time and its error for each value of the width a profile off the width distribution is made. Fitting this function with two third degree polynomials gives the time correction function $f(W)$. In some cases 1 or 3 fits can also be used to increase the accuracy of the time correction. This is showed in figure 27. The corrected time distribution can then be calculated as:

$$time = \begin{cases} width < 15.7 & t_{start} - t_{stop} - f1(W) \\ width > 15.7 & t_{start} - t_{stop} - f2(W) \end{cases}$$

The time distribution for 400MHz frequency and 100mV (10% of signal amplitude) noise amplitude, before and after time correction, is shown in figure 28.

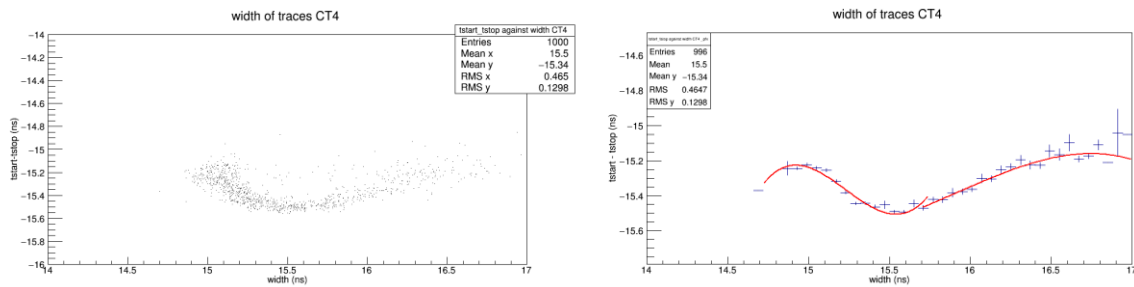


Figure 27 profile and fit of time correction function

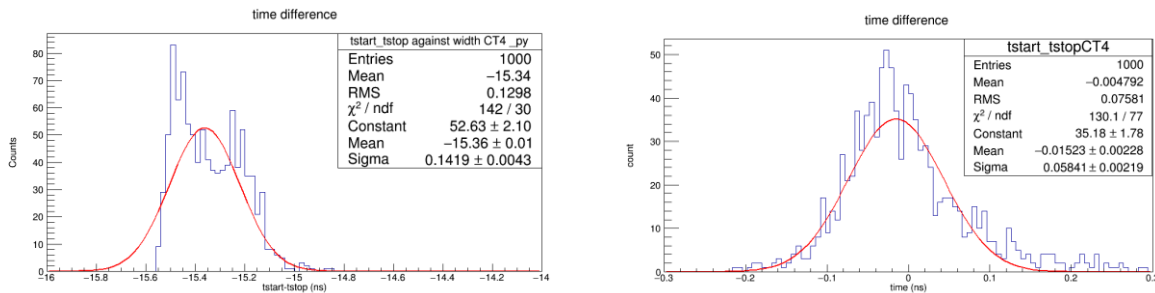


Figure 28 Time distribution of 100mV (10% of signal amplitude) noise amplitude and 400MHz frequency before (left) and after (right) time correction

Results

To determine the accuracy of the simulation the amplitude of the primary signal with noise of the simulation and experiment is compared. The amplitude of the primary signal with noise is taken with a varying frequency from 0-1GHz in steps of 50MHz. The results are shown in figure 29. The black points are the experimental data and the red points are the simulated data. Within the error bars the simulated and experimental data agree, so the results can be trusted.

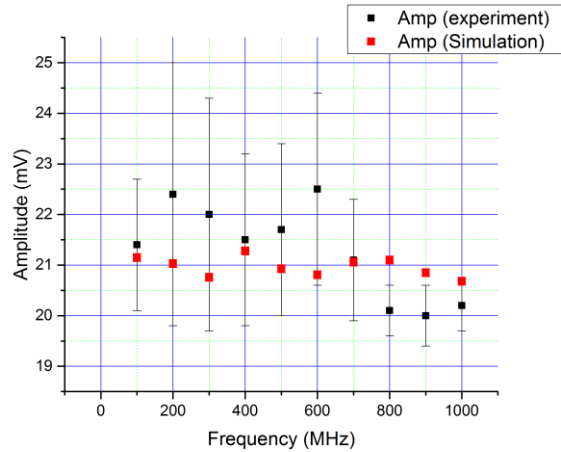


Figure 29 Amplitude of the signal with noise taken from the experiment (black) and the simulation (Red)

Below 400MHz the NINO amplifier could not distinguish between the noise and the signal and it rendered the NINO amplifier unstable. This means that the signal coming from the NINO chip could only be investigated between 400MHz-1GHz. Comparing the amplitude of the primary signal with noise and the amplitude of the noise, the noise amplitude as a percentage of the primary signal is calculated and the results are shown in figure 30.

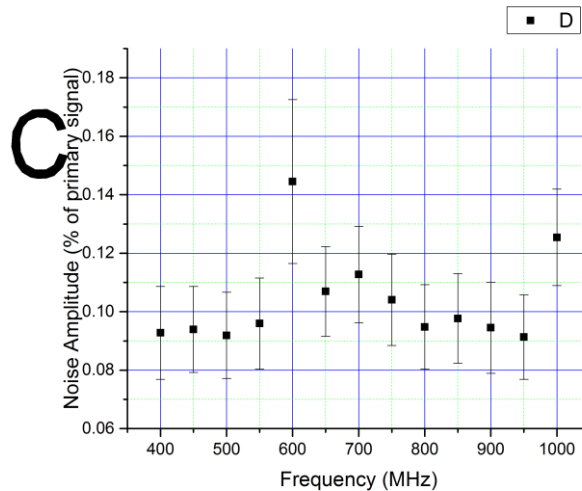


Figure 30 Noise amplitude as a percentage of the primary signal

Figure 30 shows that the noise amplitude is about 10% of the signal amplitude within the error bars. The noise amplitude stays mostly constant when varying the frequency. Varying the frequency from 400MHz to 1GHz in steps of 50MHz the variance of the corrected time distribution is calculated and shown in Figure 30. The measured variance is $\sigma_{total}^2 = \sigma_{NINO}^2 + \sigma_{noise}^2 + \sigma_{oscilloscope}^2$. The $\sigma_{oscilloscope}$ is 1-2ps and can be ignored. The σ_{noise} (red points) is calculated by the simulation so σ_{NINO} (blue) can easily be calculated by $\sigma_{NINO} = \sqrt{\sigma_{total}^2 - \sigma_{noise}^2}$.

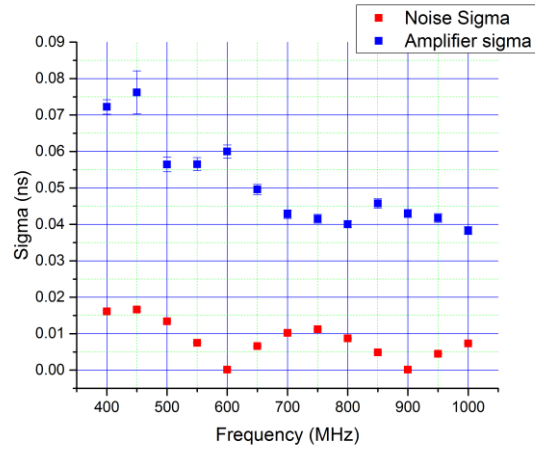


Figure 31 Variance of time distribution for the noise variance (red) and the NINO amplifier variance (blue)

The variance introduced by the NINO chip without noise is 39ps. Above 700MHz the impact of the noise is minimal and at 1000MHz the noise seems to have no impact on the variance at all. Below 700MHz however something seems to have a big impact on the variance of the NINO chip. A maximum value of 76ps at 450MHz is found for the variance of the NINO chip, almost double the variance without noise. Since the variance introduced by the noise at 450MHz is only 16ps it does not constitute an increase of 36ps in the variance. The variance must come from somewhere else. The time jitter of the differential splitter should be between 1-2ps, but was measured to be 37ps, meaning that the noise has an overall low impact on the time distribution variance. This does not explain why time jitter in the differential splitter is observed only below 700MHz. The large time jitter of the differential splitter could be due to the fact that the noise is added to the power supply of the differential splitter. The variance introduced by the electrical circuits seems to have a much larger impact than the variance introduced by the noise, however due to the high time jitter this is uncertain.

A period of 200MHz can be observed, this means that a 5ns interval is integrated over when determining the width and charge of the pulse and not a 3ns interval as used in the simulation. It can also be seen in figure 31 that the variance is less for higher frequency as observed in the simulation.

Conclusion

The structures seen in the time and width distributions in figures 12 and 14 is not observed in the experimental situation, see figure 28. The variance of the time distribution for white noise is constant around 3ps for 50% noise and 0.6ps for 10% noise. This is small enough to be ignored in an experimental situation where the electrical circuits will introduce a higher variance.

For 50% sinusoidal noise the variance can have a maximum value of 27ps and for 10% noise the maximum value is 15ps at a frequency of 50MHz according to the simulation. In the simulation a 300MHz period was observed due to the 3ns integration range. In the experiment a 200MHz period was observed due to the 5ns integration range. It can also be seen that higher frequencies of noise has a smaller impact on the time resolution. Experimentally the NINO amplifier was unstable for all frequencies below 400MHz. The maximum variance introduced by the NINO amplifier and differential splitter is 76ps at 450MHz, while the noise is only 16ps at 450MHz according to the simulation. The variance introduced by the noise seems to be small in comparison to the variance introduced by the NINO amplifier and differential splitter, however due to the high time jitter (37ps) of the differential splitter this result has a high uncertainty. A different way of coupling the noise to the signal should be used to experimentally confirm this.

References

1. A.N. Sissakian, *et al.*, .The MultiPurpose Detector (MPD), Conceptual Design Report, v1.4, http://nica.jinr.ru/files/CDR_MPD/MPD_CDR_en.pdf
2. Kh.U. Abraamyan, *et al.*, Nucl. Instr. Meth. **A628** (2011) 99.
3. V.A. Babkin, *et al.*, MPD NICA Technical Design Report of the Time of Flight System (TOF)
4. Tatsuya Chujo, PHENIX TOF Upgrade Project, Vanderbilt university, online at: www.phenix.bnl.gov/WWW/publish/chujo/presentation/CAARI2004_chujo.ppt mrpc detector
5. F. Anghinolfi, *et al*, Nucl. Instr. Meth. **A533** (2004) 183.
6. R.Becker, et. Al., Nuclear Instruments and Methods in Physics Research Section A 377 (1996) 459
7. F. Gonnella, et. Al., Nuclear Instruments and Methods in Physics Research A 791 (2015) 16-21
8. E. Usenko, ASIC NINO2003 Test results, 2003
9. M.C Jeruchim, P.Balaban, K.S. Shanmugan, 2002, *Simulation of Communication Systems*, 2nd edition, Kluwer academic publishers.
10. S.M Ross, 2010, *A first course on Probability*, 8th edition, Pearson education.
11. "Proportional counter avalanches" by Dougsim - Own work, online at: https://commons.wikimedia.org/wiki/File:Proportional_counter_avalanches.jpg#/media/File:Proportional_counter_avalanches.jpg